ADVANCED ENERGY MATERIALS
www.advenergymat.de

High-Performance Ta_2O_5/Al-Doped Ag Electrode for Resonant Light Harvesting in Efficient Organic Solar Cells

*Dewei Zhao, Cheng Zhang, Hyunsoo Kim, and L. Jay Guo**

A efficient indium tin oxide (ITO)-free transparent electrode based on an improved Ag film is designed by introducing small amount of Al during co-deposition, producing ultrathin and smooth Ag film with low loss. A transparent electrode as thin as 4 nm is achieved by depositing the film on top of Ta_2O_5 layer, and organic solar cells based on such ultrathin electrode are built, producing power conversion efficiency over 7%. The device efficiency can be optimized by simply tuning Ta_2O_5 layer thickness external to the organic photovoltaic (OPV) structure to create an optical cavity resonance inside the photoactive layer. Therefore Ta_2O_5/Al-doped Ag films function as a high-performance electrode with high transparency, low resistance, improved photon management capability and mechanical flexibility.

1. Introduction

Organic solar cells (OSCs) have been studied extensively, potentially as a future photovoltaic (PV) technology for clean energy production by their low cost, mechanical flexibility, large scale fabrication, and light weight.[1–8] Power conversion efficiencies (PCEs) of OSCs have been boosted to 10% or higher, making this technology more promising than ever.[9–11]

For OSCs, transparent, conductive, and mechanically flexible electrodes are desired, which are not easily satisfied by the most commonly used indium tin oxide (ITO) electrode.[12] Therefore, many alternatives have been developed until now, among which silver (Ag) based electrode is promising due to its high conductivity and improved mechanical stability on flexible substrates compared to ITO.[13–26] Ag usually forms two types of electrodes: nanostructures and planar thin films.

Ag nanostructures, such as mesh structures and nanowire networks,[17,27,28] can be achieved by complex fabrication process and they have advantages of high transmittance and relatively low sheet resistance. However, it is difficult to be defect-free over a large area and regions between the wires are not conducting and can not collect charges unless an additional conductive layer is added.[18] Compared with nanostructures, planar thin Ag films can be easily prepared without defects over a large area and potentially applied to semitransparent windows and tandem architectures.[29] Moreover, to further boost the device efficiency, a resonant optical cavity can be created between the transparent thin Ag film and an opaque back contact metal electrode, thus trapping light inside the active layer and enhancing its light absorption.[22] However, Ag follows 3D growth mode: during deposition, Ag atoms first agglomerate into isolated islands, and as the deposition continues, these islands finally connect to each other and form a continuous film.[30] On one hand, a certain threshold of thickness (usually beyond 10 nm) is required to get a continuous and conductive Ag film. Though the conductivity is satisfied by a thicker film, the transparency is inevitably compromised. On the other hand, the roughness of a continuous Ag film is large (e.g., root-mean-square (RMS) roughness of 6 nm for 15 nm Ag film),[30] resulting in additional light scattering loss. Moreover, since most OSCs are only few hundred nm thick, a rough surface could easily result in electrical shorts between electrodes, especially for large-area devices. To address the issues mentioned above, a wetting layer is usually placed underneath the Ag film to promote the formation of continuous films below or around 10 nm. Thus far, various wetting layers have been demonstrated by either dielectric materials (MoO_x,[22,24,31–33] ZnO,[34] WO_3,[35] and TeO_2[36]) or semiconductors/metals (Ge[30] and Au[37]). Semiconductors and metals are lossy in the visible band, leading to the reduced transparency. Besides the use of wetting layers, thin and smooth Ag films have also been achieved by treating the substrate with a layer of molecules to promote the Ag nucleation[38] or cooling down the substrate temperature during the Ag deposition.[22] However, it is highly desirable to have an alternative, simpler, and more scalable method to fabricate thin and smooth Ag films in a single step and without special treatment of the substrate or special control of the deposition condition.

We recently reported an ultrathin and smooth Ag film without any wetting layer, achieved by doping small amount of Al into Ag during the film deposition.[39] In this work, we will demonstrate a conductive and transparent Ag based film as thin as 4 nm by adding a wetting layer (Ta_2O_5) underneath the Al-doped Ag. OSCs built on such thin films produce a PCE over 7%. In addition, the Ta_2O_5 layer functions as an optical

Dr. D. Zhao,[+] C. Zhang, H. Kim, Prof. L. Jay Guo
Department of Electrical Engineering
and Computer Science
University of Michigan
Ann Arbor, MI 48109, USA
E-mail: guo@umich.edu
[+]Present address: Department of Physics and Astronomy, and Wright Center for Photovoltaics Innovation and Commercialization, University of Toledo, Toledo, OH 43606, USA

DOI: 10.1002/aenm.201500768

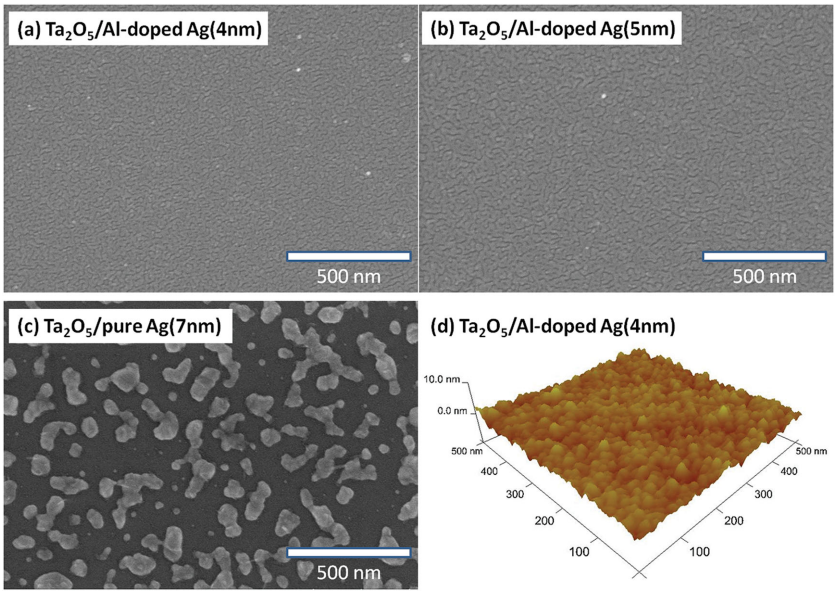

Figure 1. SEM images of a) Ta_2O_5/Al-doped Ag (4 nm), b) Ta_2O_5/Al-doped Ag (5 nm), c) Ta_2O_5/pure Ag (7 nm), and d) AFM image of Ta_2O_5/Al-doped Ag (4 nm) with an RMS roughness of 0.76 nm. All films are deposited on fused silica substrates. The scale bar for SEM images is 500 nm.

spacer to tune the optical field distribution in the entire solar cell without the need to change the other layers' geometries, locating the optical cavity resonance inside the active layer. The light harvesting of the active layer is enhanced in a certain range of its absorption spectrum while the absorption in the rest of the spectrum is not sacrificed (improved photon management), leading to enhanced PCEs. Moreover, devices fabricated on Ta_2O_5/Al-doped Ag electrodes have superior bending capability over ITO-based ones. Our work suggests that Ta_2O_5/Al-doped Ag films act as a high-performance electrode for OSCs with high transparency, low resistance, and improved photon management capability.

2. Results and Discussion

Ag tends to grow as isolated islands due to the Volmer–Weber growth mode.[40] In previous work, we have demonstrated that a Ag film as thin as 6 nm without any wetting layer can be achieved by doping a small amount of Al during Ag deposition.[39] The doped Al atoms contribute to an enhanced density of nucleation sites on the substrate, which facilitates the growth of continuous thin Ag films with a smooth morphology (e.g., RMS roughness of 0.82 nm for a 6 nm film).[41] Dielectric materials, such as MoO_x[22] and TeO_2,[36] are known to promote continuous Ag film formation. Extending this approach, Ta_2O_5 is employed in this work as a wetting layer to further reduce the percolation threshold of a continuous Al-doped Ag film. Compared with 6 nm Al-doped Ag film directly on fused silica substrates, the insertion of Ta_2O_5 layer allows a continuous film formation down to 4 nm. **Figure 1**a,b show the scanning electron microscopy (SEM) images of 4 and 5 nm Al-doped Ag film on a 10 nm Ta_2O_5 layer. The film is continuous and has a uniform morphology, which is also confirmed by the atomic force microscope (AFM) image in Figure 1d (for 4 nm film). The RMS roughness of 4 nm and 5 nm Al-doped Ag on Ta_2O_5 is 0.76 and 0.72 nm (see Figure S1, Supporting Information), respectively. In sharp contrast, 7 nm pure Ag on Ta_2O_5 is still discontinuous and consists of isolated islands (Figure 1c).

Figure 2a shows the transmittance spectra of Ta_2O_5(10 nm)/Al-doped Ag films with varying Al-doped Ag layer thickness from 4 to 7 nm. The deposition of all Al-doped Ag films has the calibrated rates of Al at 0.06 nm s^{-1} and Ag at 0.9 nm s^{-1}, according to previously characterized optimal condition.[39] Films with less than 7 nm exhibit flat and averaged 75% transmission in the entire range. It is worthy to note that the 7 nm film has higher transmission than thinner films. This is because thinner films have more defects at an early stage of the continuous film formation and thereby larger optical loss. For the application of such ultrathin films as electrodes in OSCs, 40 nm ZnO as electron transport layer (ETL) is spin-coated onto Ta_2O_5 (10 nm)/Al-doped Ag films. Adding a ZnO layer further increases the transmittance of such electrodes in the entire spectrum, especially for the 7 nm Al-doped Ag whose

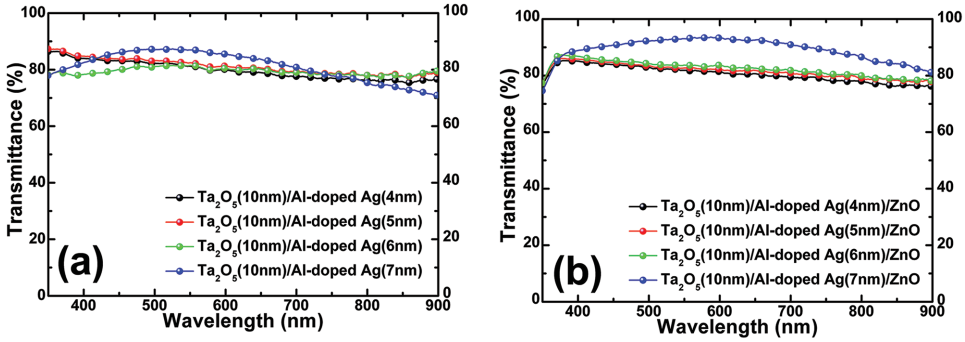

Figure 2. Transmittance spectra of a) Ta_2O_5/Al-doped Ag (4, 5, 6, and 7 nm), b) Ta_2O_5/Al-doped Ag (4, 5, 6, and 7 nm)/ZnO (40 nm). All films are deposited on fused silica substrates.

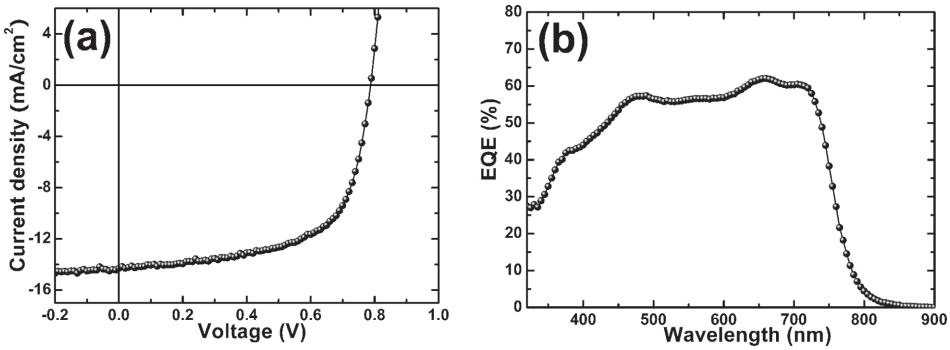

Figure 3. a) *J–V* characteristic and b) EQE spectrum of Ta_2O_5/Al-doped Ag (4 nm) as electrode-based cell.

transmission is promoted to be 93% at 550 nm (Figure 2b). This can be explained that ZnO acts as an antireflection coating.[39] The sheet resistances of Ta_2O_5 (10 nm)/Al-doped Ag (4, 5, 6, and 7 nm) are 46.8, 33.8, 30.1, and 23.1 Ω sq^{-1}, respectively, suitable for the application in OSCs.

An ultrathin Ag film down to 4 nm is already applicable in making high-performance solar cells. **Figure 3**a shows the *J–V* characteristic of the device with Ta_2O_5/Al-doped Ag (4 nm) as the electrode and poly[4,8-bis(5-(2-ethylhexyl)thiophen-2-yl)-benzo[1,2-b;4,5-b′]dithiophene-2,6-diyl-alt-(4-(2-ethylhexanoyl)-thieno[3,4-b]thiophene-)-2–6-diyl)] (PBDTTT-C-T):[6,6]-phenyl C71-butyric acid methyl ester ($PC_{70}BM$) as the photoactive layer. The device geometry is shown in **Figure 4**d. The device with 4 nm Al-doped Ag has a PCE of 7.11% with a short-circuit current density (J_{sc}) = 14.3 mA cm^{-2}, open-circuit voltage (V_{oc}) = 0.79 V, and fill factor (FF) = 62.9%. Its corresponding EQE spectrum is shown in Figure 3b, exhibiting broad spectral response with a peak EQE of 62% at 655 nm. To the best of our knowledge, it is the thinnest Ag layer as electrode in efficient OSCs. Our results indicate that a 4 nm Al-doped Ag film is continuous and conductive to produce identical V_{oc} to the ITO control device and also a reasonable FF.[39]

Next we demonstrate that the PCE of an OSC device can be optimized through the resonant light harvesting by adjusting the Ta_2O_5 layer thickness. Although PCE is highly correlated to light absorption in the active layer, increasing its thickness is a straightforward way to increase the light absorption but not always an efficient approach to boost PCE. This is due to

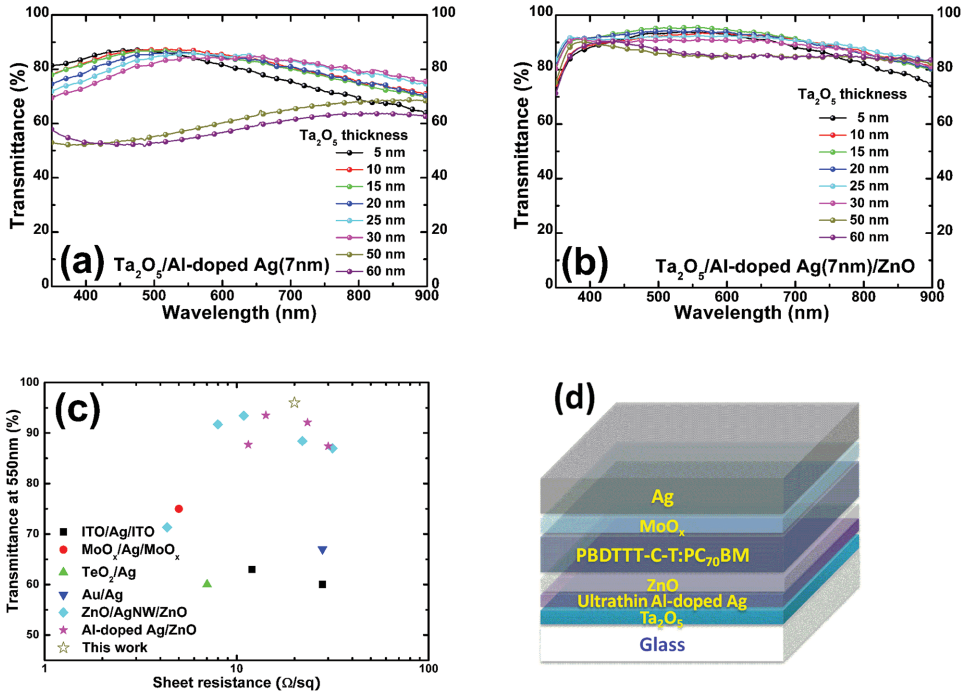

Figure 4. Transmittance spectra of a) Ta_2O_5 (x nm)/Al-doped Ag (7 nm) and b) Ta_2O_5 (x nm)/Al-doped Ag (7 nm)/ZnO (40 nm) with varying thickness of Ta_2O_5 layer. c) Comparison of optical transmittance (at 550 nm) versus sheet resistance of our work Ta_2O_5/Al-doped Ag/ZnO with other reported results based on Ag planar films/nanostructures: ITO/Ag/ITO,[50] MoO_x/Ag/MoO_x,[32] TeO_2/Ag,[36] Au/Ag,[37] ZnO/AgNW/ZnO,[51] Al-doped Ag/ZnO,[39] in which all selected data are based on their applications in optoelectronic devices. d) Schematic of the OSC devices with Ta_2O_5/Al-doped Ag as electrode.

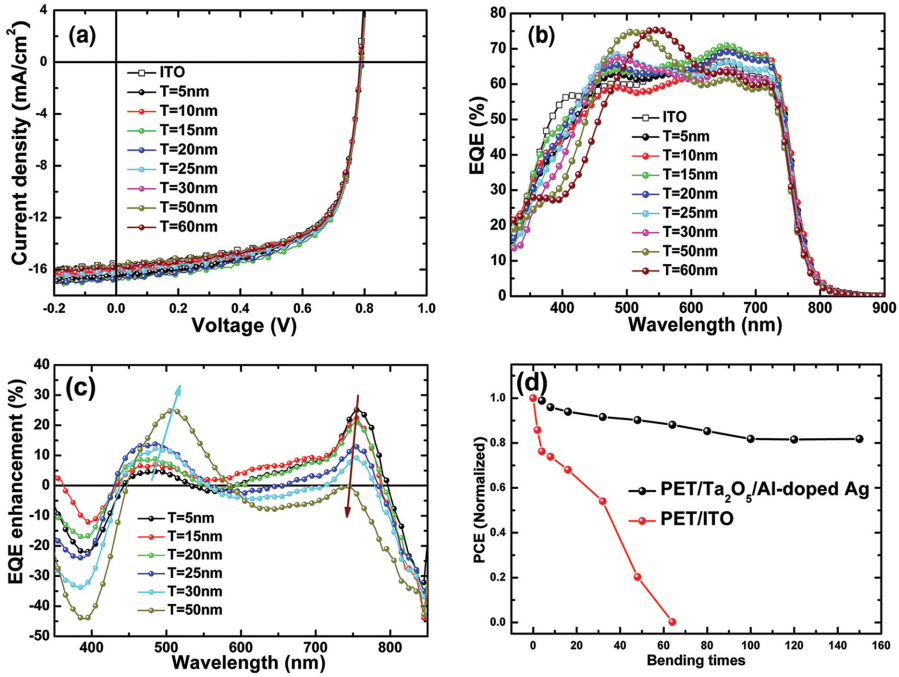

Figure 5. a) *J–V* characteristics and b) EQE spectra of ITO and Ta_2O_5 (x nm)/Al-doped Ag (7 nm) electrode-based OPVs. c) EQE enhancement of Ta_2O_5 (5, 15, 20, 25, 30, and 50 nm)/Al-doped Ag (7 nm) based OPVs over ITO-based one. d) Bendability test of the devices with PET/ITO and PET/Ta_2O_5 (15 nm)/Al-doped Ag (7 nm) as electrodes with bending times.

the short exciton diffusion length and low carrier mobility in organic semiconductors, which result in high recombination rate of the photogenerated charge carriers during transport toward the electrodes before being extracted. The above physical limitations indicate that a relatively thin photoactive layer is desired, as long as the light absorption efficiency is not compromised at the same time.[7,42–45] To achieve this goal, light trapping plays an important role in obtaining strong light absorption without relying on increasing the photoactive layer thickness. By choosing a proper Ta_2O_5 layer thickness, an optical field resonance is formed between top and bottom electrodes and it contributes to the enhanced light field inside the active layer.

The transmittance spectra of Ta_2O_5/Al-doped Ag (7 nm) with varying Ta_2O_5 thickness are shown in Figure 4a. It can be seen that the transmittance peak shifts toward the longer wavelength with the increase of Ta_2O_5 thickness from 5 to 30 nm. Beyond the peak, the transmittance gradually decreases with wavelength due to the increase of the reflection of Al-doped Ag film in the near-infrared (NIR) range, as is true for good metals.[22,39] Coating a ZnO layer on top further increases the transmittance, as shown in Figure 4b. The transmittance becomes higher and flatter in the range of 400–800 nm. For example, the maximum transmittance is 96% at 550 nm for Ta_2O_5 (15 nm)/Al-doped Ag (7 nm)/ZnO (40 nm) film. Figure 4c shows the comparison of optical transmittance (at 550 nm) versus sheet resistance of our work (Ta_2O_5/Al-doped Ag/ZnO) with other reported works based on thin Ag planar films or nanostructures, where our work shows better or comparable performance.

To evaluate the effect of Ta_2O_5/Al-doped Ag electrode on the resonant light harvesting, solar cells using PBDTTT-C-T:$PC_{70}BM$ were built up on such electrodes. As a comparison, ITO is used as the electrode in the control device. Figure 4d shows the device geometry using ITO and Ta_2O_5/Al-doped Ag electrodes with Ta_2O_5 thickness varying from 5 to 60 nm. 40 nm ZnO was first coated on all electrodes as ETL, and 70 nm PBDTTT-C-T:$PC_{70}BM$ layer was spin-coated subsequently with the same solution concentration and spinning speed. Finally, the top electrode was finished with 10 nm MoO_x and 100 nm Ag.

Figure 5a shows the comparison of the *J–V* characteristics of devices whose electrodes are either ITO or Ta_2O_5/Al-doped Ag (7 nm) with varying thickness of the Ta_2O_5 layer. Their main photovoltaic parameters are tabulated in **Table 1**. The ITO-based device has a PCE of 8.22% with a J_{sc} = 15.54 mA cm^{-2}, V_{oc} = 0.79 V, and FF = 66.9%. Device built on Ta_2O_5 (15 nm)/Al-doped Ag (7 nm) has a PCE of 8.57% with a J_{sc} = 16.92 mA cm^{-2}, V_{oc} = 0.79 V, and FF = 64.1%. All devices have identical V_{oc}s, indicating that no voltage loss occurs at either the anode or the cathode electrodes for both ITO and Ta_2O_5/Al-doped Ag (7 nm) with the help of interfacial layers: MoO_x[46,47] and ZnO.[46] Meanwhile, since Ta_2O_5 layer is the outmost layer of the entire device and only works as an optical spacer rather than a charge transport layer, changing its thickness would not affect the electrical performance of the devices. The FFs of ITO and Ta_2O_5/Al-doped Ag (7 nm) based devices are comparable, due to good contacts of ITO and Ta_2O_5/Al-doped Ag (7 nm) with the ZnO layer. Therefore, the increased PCE of Ta_2O_5/Al-doped Ag based devices primarily results from the enhancement of J_{sc}.

Figure 5b shows the external quantum efficiencies (EQEs) of the devices with ITO and Ta_2O_5/Al-doped Ag (7 nm) with varying thickness of the Ta_2O_5 layer. Their spectral responses reflect the capability of converting photons to electrons at a certain wavelength. For instance, the EQE-integrated J_{sc} for the ITO-based device is 14.8 mA cm^{-2}, while that for the Ta_2O_5 (15 nm)/Al-doped Ag (7 nm) based device is 15.8 mA cm^{-2}.

Table 1. Summary of performance metrics of the devices with ITO and Ta_2O_5/Al-doped Ag (7 nm) with varying thickness of Ta_2O_5 layer, which are obatined from six devices for each condition.

	J_{SC} [mA cm^{-2}]	V_{oc} [V]	FF [%]	PCE [%]
ITO control	15.54 (±0.20)	0.79 (±0.01)	66.9 (±0.4)	8.22 (±0.18)
Ta_2O_5 = 5 nm	16.43 (±0.24)	0.79 (±0.01)	63.2 (±0.3)	8.20 (±0.20)
Ta_2O_5 = 10 nm	16.17 (±0.15)	0.79 (±0.01)	64.8 (±0.5)	8.28 (±0.19)
Ta_2O_5 = 15 nm	16.92 (±0.19)	0.79 (±0.01)	64.1 (±0.6)	8.57 (±0.22)
Ta_2O_5 = 20 nm	16.63 (±0.20)	0.79 (±0.01)	64.4 (±0.3)	8.46 (±0.18)
Ta_2O_5 = 25 nm	16.40 (±0.10)	0.79 (±0.01)	65.0 (±0.5)	8.42 (±0.17)
Ta_2O_5 = 30 nm	15.75 (±0.16)	0.79 (±0.01)	66.3 (±0.2)	8.25 (±0.16)
Ta_2O_5 = 50 nm	15.68 (±0.15)	0.79 (±0.01)	66.3 (±0.1)	8.21 (±0.15)
Ta_2O_5 = 60 nm	15.81 (±0.23)	0.79 (±0.01)	66.3 (±0.2)	8.28 (±0.21)

The spectral response of Ta_2O_5/Al-doped Ag (7 nm) based devices is different from that of ITO-based device, where the former exhibits significant enhancement in certain wavelength ranges over the ITO-based device. Specifically, the EQE enhancements for selected thickness of Ta_2O_5 layer (5, 15, 20, 25, 30, and 50 nm) are shown in Figure 5c. For all cases except 50 nm Ta_2O_5, Ta_2O_5/Al-doped Ag (7 nm) based devices have two enhanced EQE regimes compared to the ITO-based one. With the increase of the Ta_2O_5 layer thickness, the enhancement at shorter wavelength gets more prominent, while the other one at longer wavelength becomes weaker. It is worth noting that the 15 nm Ta_2O_5 device obtains a consistently enhanced EQE from 430 to 780 nm compared with ITO-based device, leading to the strongest photocurrent enhancement and the highest PCE among all devices.

To verify the origin of the EQE enhancement in the Ta_2O_5/Al-doped Ag (7 nm) based devices, we simulate the optical field intensity ($|E|^2$) distribution versus position and wavelength by the 1D transfer matrix method,[48,49] since light absorption and photocurrent generation in the active layer are strongly correlated with the optical field intensity. The light is incident normally into the glass substrate and the optical field intensity $|E|^2$ inside the solar cell is normalized to the incoming field intensity. The field intensity profiles inside ITO-based device and Ta_2O_5 (15 nm)/Al-doped Ag (7 nm) based one are shown in **Figure 6**a,b. There is a strong field enhancement ranging

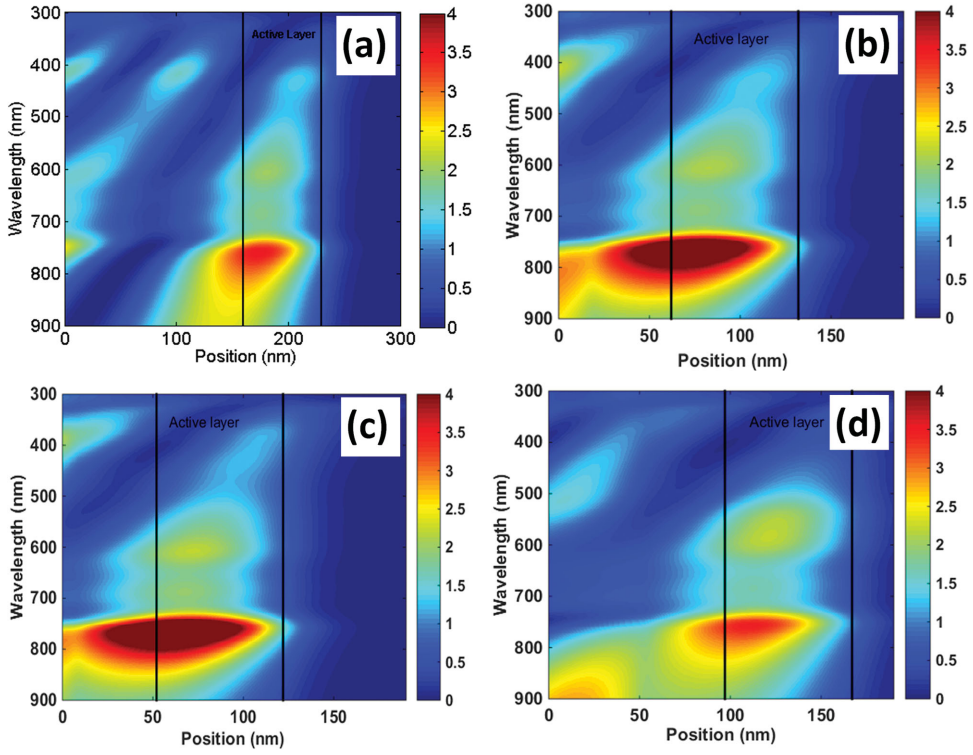

Figure 6. Simulation of the optical field intensity ($|E|^2$) distribution versus position and wavelength in a) ITO-based device, b) Ta_2O_5 (15 nm)/Al-doped Ag (7 nm) based device, c) Ta_2O_5 (5 nm)/Al-doped Ag (7 nm) based device, and d) Ta_2O_5 (50 nm)/Al-doped Ag (7 nm) based device.

from 750 to 850 nm in the Ta_2O_5 (15 nm)/Al-doped Ag (7 nm) based device, and a weak field enhancement between 500 and 650 nm, in agreement with measured EQE enhancement. When the thickness of Ta_2O_5 layer increases from 5 to 50 nm, the resonance at the longer wavelength (750 to 850 nm) gets weaker, while the resonance at the shorter wavelength (500 to 650 nm) becomes stronger (Figure 6c, d). This trend is also consistent with the measured EQE. It is worth mentioning that the optical field distribution is modulated by solely varying the thickness of Ta_2O_5 layer, which is at the outmost of the entire device and does not affect the charge transport or collection. Thereby, there is no limit in the Ta_2O_5 layer thickness or any requirement on the modification of other layers in the device, making this approach universal and easy-to-apply. To further demonstrate the generality of this approach, devices using Ta_2O_5/Al-doped Ag as electrodes but with a thinner active layer (50 nm) were fabricated. Similarly, by adjusting solely the Ta_2O_5 layer thickness, the device performance can be optimized and improved as compared with the ITO control device. The measured parameters are listed in Figure S2, Supporting Information.

The thickness of the semitransparent metal electrode influences the resonance effect inside the active layer in terms of both enhanced light intensity and spectrum width, thus affecting the solar cell performance. This is demonstrated in Figure S3, Supporting Information, showing light field intensity distribution ($|E|^2$) inside the solar cell with different Al-doped Ag electrode thicknesses. The Al-doped Ag layer thickness varies among 4, 7, 10, and 14 nm, while the Ta_2O_5/ZnO/PBDTTT-C-T:$PC_{70}BM$/MoO_x/Ag layer thicknesses are fixed at 15 nm/40 nm/70 nm/10 nm/100 nm, respectively. Varying the Al-doped Ag thickness does not obviously change the resonant wavelength and location inside the device. This is because for a constructive interference to happen, the light field needs to be in phase at a certain position for a certain wavelength. The optical phase is contributed by both the propagation phase inside each layer and the reflection phase shift between layers, which are not affected too much by slightly varying the Al-doped Ag thickness in a small range. However, varying the metal electrode thickness will change its reflectance/transmittance, thus affecting the enhanced field intensity as well as its spectrum width. For a thin electrode (e.g., 4 nm), the resonance has a weak peak intensity, but a broad spectrum. When the electrode films become thicker (e.g., 7 and 10 nm), the peak intensity gets higher, but the spectrum width is compromised. If the electrode gets even thicker (e.g., 14 nm), both the peak intensity and spectrum width are reduced and this is attributed to the relatively high loss associated with the metal electrode.

To further study the effect of Al-doped Ag electrode thickness on the device performance, we simulate J_{sc} of solar cells with different Al-doped Ag electrode thicknesses while keeping the other layers unchanged. A constant internal quantum efficiency was assumed for all absorbed light.[49] Two devices with different active layer thicknesses (50 and 70 nm) are studied, consistent with our experimentally demonstrated ones. In each case, the Ta_2O_5 layer thickness is chosen to correspond to the maximum EQE (25 nm for 50 nm active layer device and 15 nm for 70 nm active layer device). The normalized J_{sc} is plotted in Figure S4, Supporting Information. For the 70 nm active layer device, the simulated current stays basically flat for thin Al-doped Ag films (<8 nm), with a maximum value at 6 nm Al-doped Ag and then starts to decrease with the increasing thickness of the metal electrode. The J_{sc} of the 50 nm active layer device has a more obvious dependence on the Al-doped Ag thickness, with a maximum value at 8 nm. Therefore, a thin, smooth, and low-loss metal electrode is advantageous for the resonant light harvesting in OSCs.

In order to examine the potential application of this film on flexible substrate, the Ta_2O_5/Al-doped Ag/ZnO film was deposited on flexible PET substrates. The radius of curvature for bending test is around 5 mm. As shown in Figure 5d, the performance of ITO-based device significantly degraded each time when it was bent, and stopped operating after bending for 60 times. In contrast, the Ta_2O_5/Al-doped Ag device has stable performance even after 150 bending cycles.

3. Conclusion

In conclusion, a high-performance Ta_2O_5/Al-doped Ag electrode for resonant light harvesting in OSCs has been demonstrated. Ta_2O_5 acts as a wetting layer to assist an ultrathin, continuous, and low-loss Al-doped Ag film growth. Al-doped Ag as thin as 4 nm is achieved and works well as an electrode in efficient OSCs. By varying the Ta_2O_5 layer thickness, an optical resonant cavity can be formed within the solar cell with enhanced optical field inside the active layer. Therefore, devices with incorporated Ta_2O_5 have improved PCEs due to the significant enhancement in photocurrent through this strong resonant light trapping. Using an ultrathin and low-loss transparent electrode further benefits this light harvesting. The Ta_2O_5/Al-doped Ag electrode shows excellent flexibility compared with its ITO counterpart. Our work demonstrates Ta_2O_5/Al-doped Ag as a promising electrode for efficient thin-film OSCs.

4. Experimental Section

Film Deposition: Ta_2O_5 was deposited by RF sputtering on fused silica substrates (Kurt J. Lesker Co.). The Al-doped Ag films were co-sputtered by a DC magnetron sputter tool (Kurt J. Lesker Co.) with Argon gas at room temperature. Before loading into the chamber, the fused silica substrates were cleaned with acetone and isopropyl alcohol. The chamber base pressure was pumped to a base pressure of 1×10^{-6} Torr. During the deposition, the Argon gas pressure was 4.5 mTorr and the substrate holder was rotated at 10 rpm. Pure Ag and Al targets were cosputtered to create the ultrathin Al-doped Ag film. The film here was fabricated with 300 W Ag and 200 W Al target power for its better conductivity and transparency. The calibrated Ag deposition rate was 0.9 nm s^{-1} and Al deposition rate was 0.06 nm s^{-1}. These slow deposition rates allow accurate control of the film thickness.

Film Characterization: The thicknesses of Al-doped Ag films were calculated based on the calibrated deposition rates, being subsequently confirmed by the spectroscopic ellipsometry measurement (J. A. Woollam M-2000). Refractive index of Ta_2O_5 and Al-doped Ag were measured by spectroscopic ellipsometry, as shown in Figure S5, Supporting Information. The sheet resistance was measured by Miller FPP-5000 4-Point Probe. The transmittance spectra were recorded using UV–vis-NIR spectrometer with a bare fused silica substrate as the reference. SEM (Hitachi SU8000) and tapping mode AFM (Veeco NanoMan) were used to characterize the surface topography of films on fused silica substrate.

Device Fabrication: Control devices were fabricated on ITO-coated glass substrates with a sheet resistance of 12 Ω sq^{-1}. The substrates were cleaned in an ultrasonic bath with acetone and isopropyl alcohol for 10 min. The ITO surface was cleaned by oxygen plasma for 100 s. After sputtering, the Ta_2O_5/Al-doped Ag films and ITO substrate were transferred into a glove box filled with N_2 for ZnO coating. ZnO sol-gel solution was prepared as reported[39,46] and was spin-coated on top of ITO and Ta_2O_5/Al-doped Ag films, followed by baking at 70 °C for 5 min. Then ZnO coated substrates were taken out of glove box and baked at 150 °C for 15 min in air, forming a 40 nm ZnO layer. After baking, the substrates were transferred into the glove box again for polymer active layer deposition. A blend solution made of poly[4,8-bis(5-(2-ethylhexyl)thiophen-2-yl)benzo[1,2-b;4,5-b']dithiophene-2,6-diyl-alt-(4-(2-ethylhexanoyl)-thieno[3,4-b]thiophene-)-2–6-diyl)] (PBDTTT-C-T) (Solarmer) and [6,6]-phenyl C71-butyric acid methyl ester ($PC_{70}BM$) (American Dye Sources Inc.) with a weight ratio of 1:1.5 in chlorobenzene (25 mg mL^{-1}) with 3 vol% 1,8-diiodooctane (DIO, Sigma-Aldrich) was spin-coated onto ITO and Al-doped Ag substrates to form an active layer. Subsequently, MoO_x (10 nm) and Ag (100 nm) were evaporated sequentially (1×10^{-6} mbar) (Kurt J. Lesker). The final cells have an isolated electrode with a diameter of 1 mm. The device architecture is shown in Figure 4d. The inverted devices in this study have a structure of ITO or Ta_2O_5/Al-doped Ag/ZnO/PBDTTT-C-T:$PC_{70}BM$/MoO_x/Ag.

Device Characterization: The current density–voltage (*J–V*) characteristics were measured using a Keithley 2400 system while illuminating the solar cells with AM1.5 G simulated sunlight generated by an Oriel Solar Simulator at an irradiation intensity of 100 mW cm^{-2}. The incident power intensity at one sun (100 mW cm^{-2}) was calibrated using a Si reference cell. The devices were measured in the atmosphere without any encapsulation. The EQE measurement was performed in a N_2 glove box and EQE spectra were obtained using light from a 200 Hz-chopped and monochromated Xenon-lamp, calibrated against a silicon solar cell.

Supporting Information

Supporting Information is available from the Wiley Online Library or from the author.

Acknowledgements

D.Z. and C.Z. contributed equally to this work. The authors acknowledge the UM-SJTU Joint Institute and NSF DMR 1120923 for the support of this work, and the technical support of Lurie Nanofabrication Facility (LNF), especially Dr. Pilar Herrera-Fierro, Mr. Brian Armstrong, Mr. David Sebastian, and Dr. Vishva Ray. The authors appreciate the support from Electron Microbeam Analysis Laboratory (EMAL), particularly Dr. Haiping Sun for the film characterization. D.Z. and C.Z. acknowledge Dr. Xin Xiao and Dr. Yuan Li for measurement and discussion.

Received: April 17, 2015
Revised: May 31, 2015
Published online:

[1] G. Li, R. Zhu, Y. Yang, *Nat. Photonics* **2012**, *6*, 153.
[2] F. C. Krebs, *Sol. Energy Mater. Sol. Cells* **2009**, *93*, 1636.
[3] C. J. Brabec, S. Gowrisanker, J. J. M. Halls, D. Laird, S. Jia, S. P. Williams, *Adv. Mater.* **2010**, *22*, 3839.
[4] X. W. Sun, D. W. Zhao, L. Ke, A. K. K. Kyaw, G. Q. Lo, D. L. Kwong, *Appl. Phys. Lett.* **2010**, *97*, 053303.
[5] D. W. Zhao, P. Liu, X. W. Sun, S. T. Tan, L. Ke, A. K. K. Kyaw, *Appl. Phys. Lett.* **2009**, *95*, 153304.
[6] D. W. Zhao, X. W. Sun, C. Y. Jiang, A. K. K. Kyaw, G. Q. Lo, D. L. Kwong, *Appl. Phys. Lett.* **2008**, *93*, 083305.
[7] A. J. Heeger, *Adv. Mater.* **2014**, *26*, 10.
[8] C. E. Small, S. Chen, J. Subbiah, C. M. Amb, S.-W. Tsang, T.-H. Lai, J. R. Reynolds, F. So, *Nat. Photonics* **2012**, *6*, 115.
[9] J. B. You, L. T. Dou, K. Yoshimura, T. Kato, K. Ohya, T. Moriarty, K. Emery, C. C. Chen, J. Gao, G. Li, Y. Yang, *Nat. Commun.* **2013**, *4*, 1446.
[10] X. Che, X. Xiao, J. D. Zimmerman, D. Fan, S. R. Forrest, *Adv. Energy Mater.* **2014**, *4*, 1400568.
[11] Z. He, B. Xiao, F. Liu, H. Wu, Y. Yang, S. Xiao, C. Wang, T. P. Russell, Y. Cao, *Nat. Photonics* **2015**, *9*, 174.
[12] O. Inganas, *Nat. Photonics* **2011**, *5*, 201.
[13] D. S. Hecht, L. B. Hu, G. Irvin, *Adv. Mater.* **2011**, *23*, 1482.
[14] L. G. De Arco, Y. Zhang, C. W. Schlenker, K. Ryu, M. E. Thompson, C. W. Zhou, *ACS Nano* **2010**, *4*, 2865.
[15] D. Y. Liu, M. Y. Zhao, Y. Li, Z. Q. Bian, L. H. Zhang, Y. Y. Shang, X. Y. Xia, S. Zhang, D. Q. Yun, Z. W. Liu, A. Y. Cao, C. H. Huang, *ACS Nano* **2012**, *6*, 11027.
[16] D. Gupta, M. M. Wienk, R. A. J. Janssen, *Adv. Energy Mater.* **2013**, *3*, 782.
[17] M. G. Kang, T. Xu, H. J. Park, X. G. Luo, L. J. Guo, *Adv. Mater.* **2010**, *22*, 4378.
[18] H. Wu, D. Kong, Z. Ruan, P.-C. Hsu, S. Wang, Z. Yu, T. J. Carney, L. Hu, S. Fan, Y. Cui, *Nat. Nano.* **2013**, *8*, 421.
[19] P.-C. Hsu, S. Wang, H. Wu, V. K. Narasimhan, D. Kong, H. Ryoung Lee, Y. Cui, *Nat. Commun.* **2013**, *4*, 2522.
[20] J.-Y. Lee, S. T. Connor, Y. Cui, P. Peumans, *Nano Lett.* **2008**, *8*, 689.
[21] F. S. F. Morgenstern, D. Kabra, S. Massip, T. J. K. Brenner, P. E. Lyons, J. N. Coleman, R. H. Friend, *Appl. Phys. Lett.* **2011**, *99*, 183307.
[22] N. P. Sergeant, A. Hadipour, B. Niesen, D. Cheyns, P. Heremans, P. Peumans, B. P. Rand, *Adv. Mater.* **2012**, *24*, 728.
[23] J. Meiss, M. K. Riede, K. Leo, *J. Appl. Phys.* **2009**, *105*, 063108.
[24] S. Schubert, M. Hermenau, J. Meiss, L. Müller-Meskamp, K. Leo, *Adv. Funct. Mater.* **2012**, *22*, 4993.
[25] B. O'Connor, C. Haughn, K.-H. An, K. P. Pipe, M. Shtein, *Appl. Phys. Lett.* **2008**, *93*, 223304.
[26] B. O'Connor, K. H. An, K. P. Pipe, Y. Zhao, M. Shtein, *Appl. Phys. Lett.* **2006**, *89*, 233502.
[27] M. G. Kang, M. S. Kim, J. S. Kim, L. J. Guo, *Adv. Mater.* **2008**, *20*, 4408.
[28] J. Krantz, T. Stubhan, M. Richter, S. Spallek, I. Litzov, G. J. Matt, E. Spiecker, C. J. Brabec, *Adv. Funct. Mater.* **2013**, *23*, 1711.
[29] A. Colsmann, A. Puetz, A. Bauer, J. Hanisch, E. Ahlswede, U. Lemmer, *Adv. Energy Mater.* **2011**, *1*, 599.
[30] L. Vj, N. P. Kobayashi, M. S. Islam, W. Wu, P. Chaturvedi, N. X. Fang, S. Y. Wang, R. S. Williams, *Nano Lett.* **2009**, *9*, 178.
[31] L. Cattin, Y. Lare, M. Makha, M. Fleury, F. Chandezon, T. Abachi, M. Morsli, K. Napo, M. Addou, J. C. Bernède, *Sol. Energy Mater. Sol. Cells* **2013**, *117*, 103.
[32] H. Jin, C. Tao, M. Velusamy, M. Aljada, Y. Zhang, M. Hambsch, P. L. Burn, P. Meredith, *Adv. Mater.* **2012**, *24*, 2572.
[33] D. T. Nguyen, S. Vedraine, L. Cattin, P. Torchio, M. Morsli, F. Flory, J. C. Bernede, *J. Appl. Phys.* **2012**, *112*, 063505.
[34] H. Han, N. D. Theodore, T. L. Alford, *J. Appl. Phys.* **2008**, *103*, 013708.
[35] X. Guo, J. Lin, H. Chen, X. Zhang, Y. Fan, J. Luo, X. Liu, *J. Mater. Chem.* **2012**, *22*, 17176.
[36] J.-F. Salinas, H.-L. Yip, C.-C. Chueh, C.-Z. Li, J.-L. Maldonado, A. K. Y. Jen, *Adv. Mater.* **2012**, *24*, 6362.
[37] T. Schwab, S. Schubert, L. Müller-Meskamp, K. Leo, M. C. Gather, *Adv. Opt. Mater.* **2013**, *1*, 921.

[38] J. Zou, C.-Z. Li, C.-Y. Chang, H.-L. Yip, A. K. Y. Jen, *Adv. Mater.* **2014**, *26*, 3618.
[39] C. Zhang, D. Zhao, D. Gu, H. Kim, T. Ling, Y.-K. R. Wu, L. J. Guo, *Adv. Mater.* **2014**, *26*, 5696.
[40] R. S. Sennett, G. D. Scott, *J. Opt. Soc. Am.* **1950**, *40*, 203.
[41] D. Gu, C. Zhang, Y.-K. Wu, L. J. Guo, *ACS Nano* **2014**, *8*, 10343.
[42] M. A. Green, S. Pillai, *Nat. Photonics* **2012**, *6*, 130.
[43] X. Li, W. C. H. Choy, L. Huo, F. Xie, W. E. I. Sha, B. Ding, X. Guo, Y. Li, J. Hou, J. You, Y. Yang, *Adv. Mater.* **2012**, *24*, 3046.
[44] L. Mueller-Meskamp, Y. H. Kim, T. Roch, S. Hofmann, R. Scholz, S. Eckardt, K. Leo, A. F. Lasagni, *Adv. Mater.* **2012**, *24*, 906.
[45] B. Niesen, B. P. Rand, P. Van Dorpe, D. Cheyns, L. Tong, A. Dmitriev, P. Heremans, *Adv. Energy Mater.* **2013**, *3*, 145.
[46] A. K. K. Kyaw, X. W. Sun, C. Y. Jiang, G. Q. Lo, D. W. Zhao, D. L. Kwong, *Appl. Phys. Lett.* **2008**, *93*, 221107.
[47] V. Shrotriya, G. Li, Y. Yao, C. W. Chu, Y. Yang, *Appl. Phys. Lett.* **2006**, *88*, 073508.
[48] P. Yeh, *Optical Waves in Layered Media*, Wiley, Hoboken, NJ **1988**.
[49] L. A. A. Pettersson, L. S. Roman, O. Inganas, *J. Appl. Phys.* **1999**, *86*, 487.
[50] J. Yun, W. Wang, T. S. Bae, Y. H. Park, Y.-C. Kang, D.-H. Kim, S. Lee, G.-H. Lee, M. Song, J.-W. Kang, *ACS Appl. Mater. Interfaces* **2013**, *5*, 9933.
[51] A. Kim, Y. Won, K. Woo, C. H. Kim, J. Moon, *ACS Nano* **2013**, *7*, 1081.